THE PROTEIN SOCIETY

NMR characterization of the conformational fluctuations of the human lymphocyte function-associated antigen-1 I-domain

Hoi Tik Alvin Leung,[1,2] Predrag Kukic,[1] Carlo Camilloni,[1] Francesco Bemporad,[1,3] Alfonso De Simone,[4] Francesco A. Aprile,[1] Janet R. Kumita,[1] and Michele Vendruscolo[1]*

[1]Department of Chemistry, University of Cambridge, Cambridge CB2 1EW, United Kingdom
[2]Biozentrum, University of Basel, Basel CH-4056, Switzerland
[3]Dipartimento di Scienze Biomediche, Sperimentali e Cliniche, Università degli Studi di Firenze, Firenze 50134, Italy
[4]Division of Molecular Biosciences, Imperial College London, London SW7 2AZ, United Kingdom

Received 30 April 2014; Revised 13 August 2014; Accepted 19 August 2014
DOI: 10.1002/pro.2538
Published online 21 August 2014 proteinscience.org

Abstract: Lymphocyte function-associated antigen-1 (LFA-1) is an integrin protein that transmits information across the plasma membrane through the so-called inside-out and outside-in signaling mechanisms. To investigate these mechanisms, we carried out an NMR analysis of the dynamics of the LFA-1 I-domain, which has enabled us to characterize the motions of this domain on a broad range of timescales. We studied first the internal motions on the nanosecond timescale by spin relaxation measurements and model-free analysis. We then extended this analysis to the millisecond timescale motions by measuring ^{15}N-^{1}H residual dipolar couplings of the backbone amide groups. We analyzed these results in the context of the three major conformational states of the I-domain using their corresponding X-ray crystallographic structures. Our results highlight the importance of the low-frequency motions of the LFA-1 I-domain in the inactive apo-state. We found in particular that α-helix 7 is in a position in the apo-closed state that cannot be fully described by any of the existing X-ray structures, as it appears to be in dynamic exchange between different conformations. This type of motion seems to represent an inherent property of the LFA-1 I-domain and might be relevant for controlling the access to the allosteric binding pocket, as well as for the downward displacement of α-helix 7 that is required for the activation of LFA-1.

Keywords: protein dynamics; allostery; signaling mechanism; NMR spectroscopy

Introduction

Integrins are transmembrane receptor proteins that play key roles in mediating the attachment and communication of cells with their environments, including other cells and the extracellular matrix.[1–5] Integrins carry out these functions by interacting with cell surface proteins, such as cadherins, cell adhesion molecules, selectins, and syndecans, and with extracellular matrix proteins, such as collagens, fibronectins, and laminins.[6,7] Lymphocyte function-associated antigen-1 (LFA-1, also known as αLβ2 or as CD11a/CD18) is a particularly important integrin in leukocytes, the cells that combat infection and disease by eliminating foreign materials and cellular debris, as well as infectious agents and cancer cells. Through its interaction with

Additional Supporting Information may be found in the online version of this article.

*Correspondence to: Michele Vendruscolo, Department of Chemistry, University of Cambridge, Cambridge CB2 1EW, United Kingdom. E-mail: mv245@cam.ac.uk

intercellular adhesion molecules, including in particular ICAM-1 (also known as Cluster of Differentiation 54), LFA-1 regulates the recruitment of leukocytes to the sites of infection or inflammation.[8–10] Like other members of the integrin family, LFA-1 carries out its function by transmitting information in two directions across the plasma membrane, in the so-called inside-out and outside-in signaling.[11,12] During the inside-out signaling, intracellular signals elicited by chemokine and T-cell receptors rapidly upregulate the ability of LFA-1 to bind to ICAM-1.[13] Conversely, during the outside-in signaling, the binding of ICAM-1 to LFA-1 triggers the transmission of signals from the extracellular space into the cytoplasm, thereby altering gene expression and cellular metabolism.[2,14]

LFA-1 is an αβ-heterodimer with a complex domain organization. It consists of an αL-subunit of 180 kDa and a β2-subunit of 95 kDa.[15] Each subunit is composed of a large N-terminal extracellular domain, a single α-helical transmembrane domain, and a short intracellular domain.[15] Among the extracellular domains, a ~190-residue inserted domain located at the extracellular αL subunit, known as the I-domain, has been implicated as a critical ICAM-1 binding site.[11,16–19] The I-domain has been the subject of many research efforts aimed at deciphering the mechanism of bidirectional signaling in LFA-1.[14,20,21]

The I-domain adopts a Rossmann-type fold with a central hydrophobic six-stranded β-sheet surrounded by seven amphipathic α-helices (Supporting Information Fig. S1). The ICAM-1 binding site is located at its upper face. The binding site is commonly known as the metal-dependent ion-adhesion site (MIDAS) because it coordinates a single Mg^{2+} ion, which is necessary to achieve a high binding affinity. In previous structural studies, it has been observed that the I-domain exists in multiple conformational states.[10,12,22] Currently, three different states, commonly referred to as the closed,[23] intermediate,[22] and open[12,22] conformations, have been characterized, each with a different structure of the MIDAS binding site and hence with different binding affinities to ICAM-1. The closed conformation has the lowest binding affinity to ICAM-1, and it is therefore considered as inactive. This conformation has been shown to exist in the apo-form of the protein (closed apo-state)[23] and when the protein is stabilized by allosteric inhibitors bound to the hydrophobic binding pocket adjacent to α-helix 7 (closed inhibitor-bound state).[24–27] The interconversion from the closed inactive conformation to the open active conformation requires the binding of ICAM-1, that is, the rearrangement of the side chains that coordinate Mg^{2+} and open the MIDAS binding site. This rearrangement in the MIDAS site is further allosterically coupled to α-helix 7 in the C-terminus via the β1–α1, β4–α5, β5–α6, and β6–α7 loops and causes a ~10 Å downward movement of α-helix 7 along the side of the I-domain. This open active conformation can be alternatively stabilized in the apo-form (open apo-state) by introducing a disulfide bond that induces a dramatic downward displacement of α-helix 7. In this open active conformation, the binding affinity to ICAM-1 increases 10,000-fold in comparison with the affinity in the closed state.[12]

In a similar fashion to the open apo-state, the so-called intermediate state of the I-domain has been stabilized in the apo-form of the protein by introducing a disulfide bond that slightly pulls α-helix 7 down the side of the domain.[22] Even though in this intermediate conformation the rearrangements of the MIDAS side chains do not take place and the MIDAS site remains closed, this state shows a 500-fold increase in the binding affinity to ICAM-1 in comparison with the affinity in the closed state.[22]

Considerable attention has been focused on the importance of the allosteric activation of the I-domain in the regulation of the outside-in and inside-out signaling.[14,20,21] To date, the structural mechanism of this activation has been almost exclusively studied by X-ray crystallography. In these studies, structures of the wild-type I-domain and its mutational variants have been obtained at various conditions, including in the closed apo-state,[23,28,29] in a closed state stabilized by allosteric inhibitors bound to the hydrophobic binding pocket adjacent to α-helix 7,[24–27] in an intermediate state stabilized by engineered disulfide bonds,[22] and in an open active state stabilized by engineered disulfide bonds,[22] antibody fragments,[13,22,30] and ICAM ligands.[31] Although a general mechanism that couples the conformation and affinity of the I-domain has been laid out in these studies, the detailed dynamics of this coupling are yet to be determined.

In the only NMR study of LFA-1 to date,[32] the solution structure of the apo I-domain has been determined from NOESY restraints. This solution structure shows structural differences in comparison with available X-ray structures, which are most prominent in the conformation of α-helix 7. Measurements of protection factors from equilibrium hydrogen exchange in the same study imply that α-helix 7 undergoes "breathing" and "segmental" motion in the apo-state that might be important for the activation of LFA-1.

Here, we extend the analysis of the allosteric coupling between the MIDAS binding site and α-helix 7 in the apoLFA-1 I-domain by a detailed study of its backbone dynamics. We report on the motions of the I-domain on a broad range of timescales. First, we study the internal motions on the fast timescale by spin relaxation measurements and model-free analysis. We then broaden this analysis

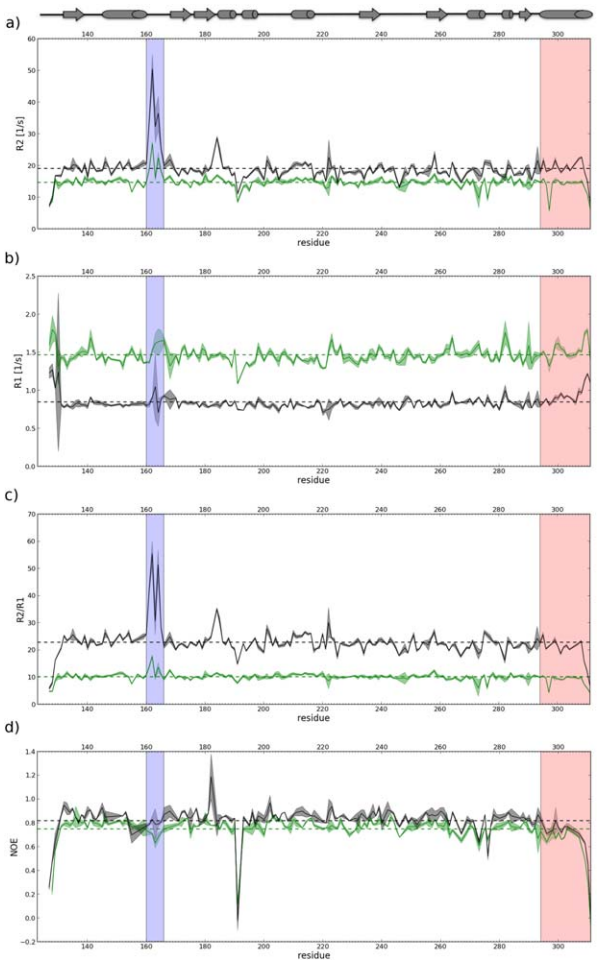

Figure 1. ^{15}N relaxation rate constants: (a) R_2, (b) R_1, (c) R_2/R_1, and (d) ^{15}N-^{1}H heteronuclear NOE data measured at 500 MHz (green) and 700 MHz (black). The α1–β2 loop region (residues 161–165) and α-helix 7 are highlighted in blue and red, respectively.

to the slow timescales by measuring ^{15}N-^{1}H residual dipolar couplings (RDCs) of the backbone amides. Finally, we analyze the results in the context of the three conformational states (closed, intermediate, and open) of the I-domain and their corresponding X-ray structures.

Results

^{15}N R_1, R_2, and NOE of the LFA-1 I-domain

Using previously assigned chemical shifts of the LFA-1 I-domain,[32] 159 and 164 nonoverlapping ^{15}N-^{1}H backbone peaks were identified at 500 and 700 MHz, respectively. The determined ^{15}N R_1, R_2, and ^{15}N-^{1}H heteronuclear NOEs are shown in Figure 1 and are listed in Supporting Information Tables S1 and S2. The data measured at 500 MHz (green curve) and 700 MHz (black curve) show similar patterns (Fig. 1).

As is commonly observed for folded proteins, the R_1 values are fairly similar throughout the sequence and only show increased variations at the two termini. The R_2 values, on the other hand, exhibit more pronounced variations along the sequence. Interestingly, however, the R_2 values of α-helix 7, which is of crucial importance for the allosteric regulation of LFA-1, are not significantly different from the overall average values of the I-domain. In addition, particularly striking is the increase in the R_2 values in the α1–β2 loop [residues 161 to 165; Supporting Information Fig. S1(b)]. The ^{15}N linewidths of these residues are also larger than the average line widths from the remainder of the ^{15}N assigned resonances. The increase of their R_2 values arises most likely from a local conformational averaging of the α1–β2 loop at a rate comparable with the chemical shift differences of the various conformational forms.

When the internal motions take place on the fast timescale, the correlation frequencies for the internal motions affect R_1 and R_2 to the same extent. Thereby, under these conditions, the R_2/R_1 ratio depends only on the overall molecular tumbling correlation time, τ_m, and can provide a useful initial estimate of the τ_m value itself.[33,34] The values of R_2/R_1 are given in Figure 1(c) and show a similar trend to the R_2 values [Fig. 1(a)]. An initial estimate of τ_m was obtained from the 10% trimmed mean of the R_2/R_1 ratio.[33] The mean R_2/R_1 values measured at 500 and 700 MHz were found to be 10.19 and 22.7, respectively, and yielded an estimate $\tau_m = 12.2$ ns. The residues for which R_2/R_1 is higher than one standard deviation are shown in Supporting Information Figure S2. The majority of the identified residues are positioned at the loop regions (Leu161-Ser165, Asp191, Glu222, Gly225, Thr267, Thr273, and Lys276) or form hydrogen bonds and hydrophobic interactions with these residues (Phe168, Ser184, and Asp185). Among three outliers, residues Lys155 and Asp297 belong to α-helices 1 and 7, respectively. These two residues are located at positions that correspond to kinks in the two α-helices according to an analysis of the secondary structure populations (Fig. 2), which were estimated from the chemical shifts using the δ2D method.[35] The last outlier, Ile258, belongs to β-strand 6 and has been speculated to be involved in the allosteric regulation of the LFA-1 I-domain.[34]

^{15}N-^{1}H heteronuclear NOE measurements, which were previously carried out by Legge *et al.*,[32] were repeated here for completeness [Fig. 1(d)]. The NOE data determined at 500 and 700 MHz show almost identical patterns and agree well with the previous results.[32] Two main observations can be made from Figure 1(d): first, residues at both termini (127–129 and 309–311) show a small decrease in NOE values in comparison with the rest of the protein; and second, Asp191, which belongs to the loop connecting α-helices 2 and 3, experiences a

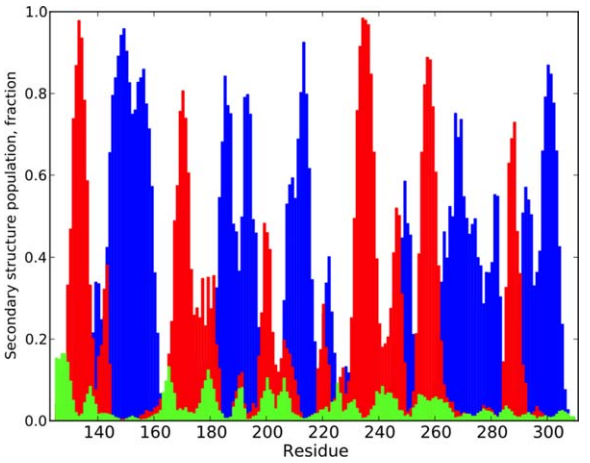

Figure 2. Secondary structure populations obtained from experimental chemical shifts using the δ2D method.[35] Secondary structure populations of β-strands are shown in red, α-helices are shown in blue, and PPII regions are shown in green.

significant decrease in the peak intensity ratio. This residue has a negative NOE value, which suggests the presence of significant contributions from rapid internal motions.

Model-free analysis

Relaxation data were analyzed by using both isotropic motion and axially symmetric motion models. As no statistically significant improvement in the axially symmetric model over the isotropic model was observed, we will only report here the results obtained from the isotropic model.

The S^2 order parameter values were simultaneously fitted using the datasets measured at 500 and 700 MHz with the Model-free 4 software.[36] The S^2 value of a residue was determined by choosing a suitable model as outlined in the work of Palmer and coworkers.[37] The optimized global value of τ_m was determined to be 12.30 ± 0.05 ns, in good agreement with the value calculated from R_2/R_1 ratio. Optimized values of the model-free parameters are reported in Supporting Information Table S3, and the sequence distribution of the S^2 values is shown in Figure 3. The overall average value of S^2 was 0.93 ± 0.07. This high value indicates the presence of restricted high-frequency fluctuations of the backbone NH vectors throughout the protein. Indeed, the S^2 values are greater than 0.8 for all residues except for the residues at the N terminus and Asp191. Furthermore, for 87% of residues, Model 1, which has only two degrees of freedom, was enough to fit the S^2 values. The S^2 values of the α-helix 7 did not again show a significant difference from the rest of the I-domain.

The S^2 values did not show any correlation with the temperature factors (B-factors) calculated from the available X-ray structures (Fig. 4). One of the reasons for the discrepancy may be the fact that B-factors are sensitive to both fast and slow timescale dynamics, whereas S^2 values are a function of rapid motions solely. On the other hand, slightly better correlation with the B-factors was observed for the R_2/R_1 outliers. For the B-factors obtained from the closed apo-state [Fig. 4(a)], a correlation was observed in the α1–β2 loop (residues 161–165) and residues Asp191, Glu222, Thr273, and Asp297. Interestingly, for the active open state [Fig. 4(c)], a correlation was observed for a larger number of sites including the α1–β2 loop, residues Lys155 and Phe168 and residues in the vicinity of the identified allosteric sites (Ile258, Thr267, Thr273, Lys276, and Asp297). Finally, there was almost no correlation between the B-factors of the closed inhibitor-bound state and the R_2/R_1 outliers [Fig. 4(b)].

RDC values of the LFA-1 I-domain

While NMR spin relaxation rates mainly describe motions on the nanosecond timescale, RDCs can be used to study motions on the millisecond timescale.[38] Therefore, to probe internal motions in the LFA-1 I-domain on these slow timescales, we measured ^{15}N-^{1}H RDCs in filamentous bacteriophage *Pf1* media.[39] The values of 135 ^{15}N-^{1}H RDCs were assigned (Supporting Information Table S4). The

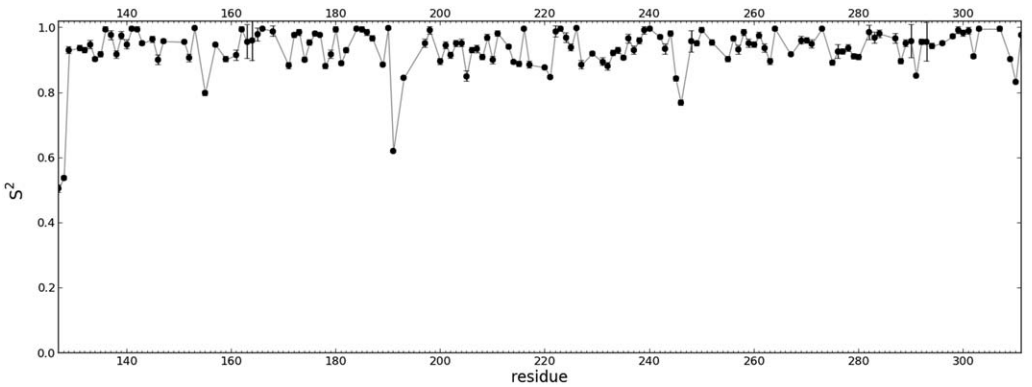

Figure 3. S^2 values of the LFA-1 I-domain fitted with the model-free approach from the relaxation data measured at 500 and 700 MHz. The average value obtained was 0.93.

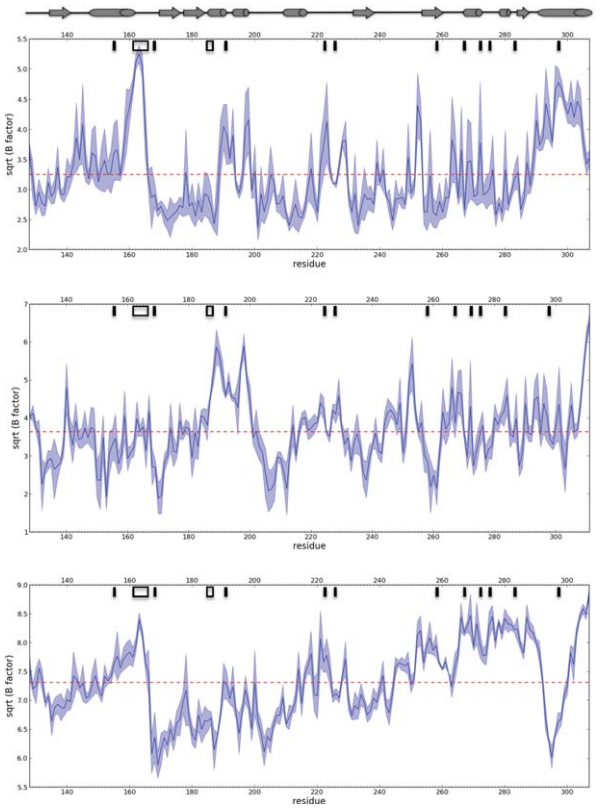

Figure 4. Residue specific $\sqrt{B}$ values of the LFA-1 I-domain obtained from the ensemble of the crystal structures of the (a) closed apo-state, (b) closed state bound to the allosteric inhibitor, and (c) open active state. The outliers of the R_2/R_1 distribution are represented by boxes and lines at the top of the figure.

measurements were repeated twice, and the errors were found to be of about 1 Hz. In *Pf1*, the maximum chemical shift perturbations of the backbone amide hydrogen and nitrogen atoms were found to be 0.1 and 0.3 ppm, respectively. Therefore, we concluded that the structure of the LFA-1 I-domain is not significantly perturbed in the presence of *Pf1* under the conditions of our experiment.

To assess the importance of the dynamics of the LFA-1 I-domain on the timescale probed by the RDC measurements, we validated the previously determined structures of the I-domain using the RDCs themselves. The level of agreement is reported using the *Q*-factor [Eq. (1)]. To predict the values of the RDCs, the magnitude and orientation of the alignment tensor relative to the molecular frame were obtained using a singular value decomposition-based method,[40] where the RDCs of residues belonging to β-strands 1, 2, 4, and 5 were used for the calculation of alignment tensors. These β-strands belong to the central β-sheet and correspond to the region with the lowest crystallographic *B*-factor in the protein [Fig. 4(a)]. The RDCs of the remaining residues were back calculated and used to determine the *Q*-factors.

The agreement between the experimentally determined RDCs and those predicted on the basis of the X-ray structure of the closed apo-state (PDB ID: 1LFA) is low, having a *Q*-factor of 0.46 [Fig. 5(a)]. This value is higher than those typical of structures of similar resolution (1.8 Å), which have *Q*-factors in the range 0.2–0.25.[41] The relatively high value of the *Q*-factor comes, at least in part, from the residues in α-helix 7, whose *Q*-factor is 0.88—a value significantly higher than those obtained for the other secondary structure elements [Fig. 5(a)]; for example, the *Q*-factor calculated for residues in the α1–β2 loop (blue) and in the MIDAS site (green) is 0.38.

To assess whether the agreement with the experimental RDCs can be improved using other conformations of the LFA-1 I-domain, we carried out the same analysis using representative structures of the closed inhibitor-bound state (PDB ID: 1CQP) and the open state (PDB ID: 3TCX). The overall *Q*-factor from the closed inhibitor-bound conformation is 0.43, whereas values 0.80, 0.87, and 0.34 are found for α-helix 7, the α1–β2 loop, and the MIDAS site, respectively [Fig. 5(b)]. Interestingly, there is almost no difference between the *Q*-factors obtained from the closed apo-state and closed inhibitor-bound state except for residues in the α1–β2 loop. This result most probably comes from the fact that residues in the α1–β2 loop in the structure with the inhibitor are closely packed against α-helix 7, unlike the case in which the inhibitor is not present. On the other hand, the *Q*-factors obtained for the open active state are significantly higher [Fig. 5(c)]. The overall *Q*-factor is 0.80, with values of 1.57, 0.87, and 0.78 for α-helix 7, residues in the α1–β2 loop, and in the MIDAS site, respectively. In the open active state, α-helix 7 is shifted down the side of the I-domain, and the MIDAS residues are in the open conformation. These conformational changes are the main reason for the increase in the *Q*-factor.

Even when ensembles of available X-ray structures from the PDB were used in fitting the alignment tensors, no improvement in the *Q*-factor was recorded. An overview of the *Q*-values calculated for different states and different regions in the protein is reported in Figure 6. The lowest value of the overall *Q*-factor was obtained from the ensembles of structures that represent the closed inhibitor-bound inactive state (*Q*-factor of 0.4) and the closed apo-state (*Q*-factor of 0.46). A higher overall *Q*-factor was found for structures in the open active state (*Q*-factor of 0.58). In addition, the only NMR structure of the apo LFA-1 I-domain in the PDB (PDB ID: 1DGQ) has a *Q*-factor of 0.76, whereas the only crystallographic structure of an apo LFA-1 I-domain variant in the intermediate state (PDB ID: 1MJN) has an overall *Q*-factor of 0.52.

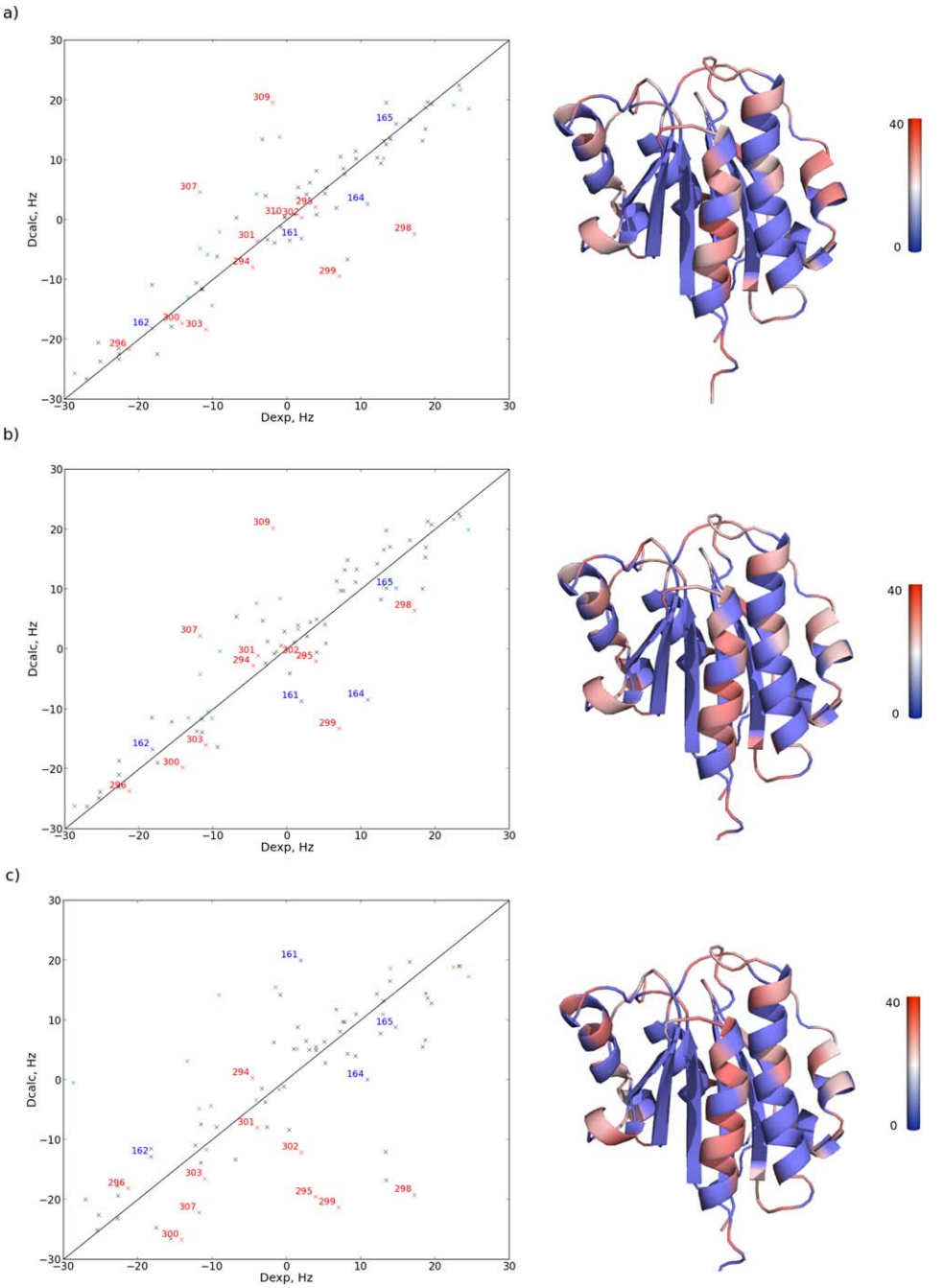

Figure 5. ^{15}N-^{1}H RDCs measured in *Pf1* at 0 m*M* NaCl concentration: (a) closed apo-state (PDB ID: 1LFA); (b) closed state bound to the allosteric inhibitor (PDB ID: 1CQP); and (c) open active state (PDB ID: 3TCX). Residues with increasing $|D_{exp}-D_{calc}|$ values are colored from blue to red. The central β-sheet was used for superimposing structures, and these residues are colored in blue.

Independently from the activation state of the I-domain, the *Q*-factors corresponding to α-helix 7, which range from 0.80 to 1.53 depending on the structure used, are consistently the highest ones among all secondary structure elements in the protein. This large discrepancy between the experimental and calculated RDCs for α-helix 7 suggests that this α-helix is likely to be highly dynamic on the timescale relevant to the RDC experiments, although it is possible that a difference between the position of this α-helix in solution and in the crystal could also play a role.

To further test these conclusions, we carried out a calculation in which we used the RDCs as conformational restraints in a single-structure refinement. The results indicate that because of the dynamics of this domain, imposing the RDC restraints on a single structure results in conformational distortions, in particular corresponding to α-helix 7 (Supporting Information Fig. S3, red box).

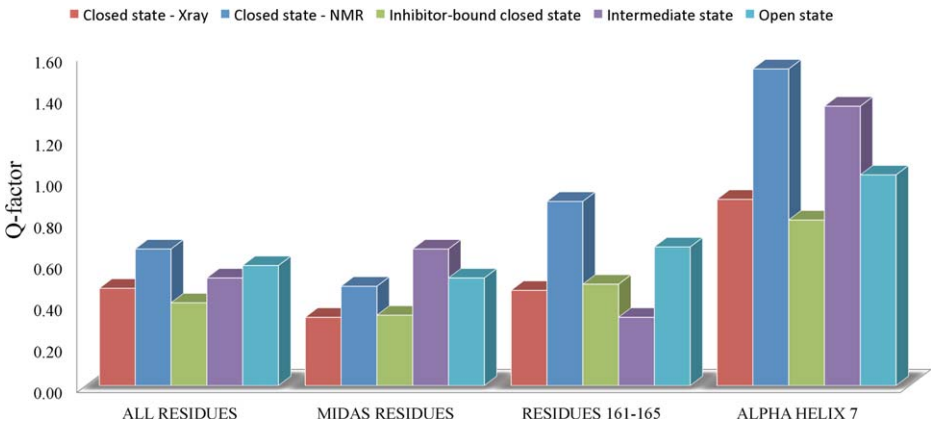

Figure 6. *Q*-factor calculated for different states and different groups of residues of the LFA-1 I-domain. The closed apo-state is represented as an ensemble of available crystallographic structures of the apo-I-domain and as an ensemble of the models from the NMR structure PDB ID: 1DGQ. The closed inhibitor-bound, intermediate, and open active states are represented by ensembles of relevant structures from PDB.

Discussion and Conclusions

The role of LFA-1 conformational changes in the bidirectional transmission of signals across the plasma membrane of leukocytes has been the object of intense scrutiny.[42,43] To date, three different conformations of the LFA-1 I-domain (closed, intermediate, and open) have been observed in X-ray structures. In all three conformations, the allosteric mechanism between the C-terminal α-helix 7 and the MIDAS residues is thought to play a central role in the bidirectional signaling process. However, a full understanding of the intrinsic dynamics of the LFA-1 I-domain and its role in the allosteric mechanism is currently still lacking.

In a previous study,[32] the backbone flexibility of the I-domain was assessed by heteronuclear ^{15}N-^{1}H NOE measured for the backbone amide groups and by hydrogen/deuterium exchange protection factors of the same groups. The reported low NOE values of α-helix 7 and their limited protection from hydrogen/deuterium exchange indicated a high flexibility of this α-helix in the closed apo-state. Such high flexibility of α-helix 7 was suggested to play an important role in LFA-1 activation.[32] Here, we have extended the analysis of the dynamics of the I-domain by studying it on timescales that have not been explored so far. In particular, we have determined R_1 and R_2 relaxation rates and further used them in the model-free analysis. In addition, we have measured the RDCs of the LFA-1 I-domain in *Pf1* and used the obtained values to validate the three conformational states observed in the X-ray structures.

Surprisingly, the S^2 values determined from the model-free analysis showed very restricted motions of the I-domain on the picosecond to nanosecond timescales. The majority of the backbone amide groups exhibited S^2 values greater than 0.9. Therefore, even though a rapid interconversion between the inactive and active states is necessary for the function of LFA-1, the motions on the picosecond to nanosecond timescales do not seem to play a crucial role in this interconversion. The only residue with an S^2 value below 0.8 was Asp191. The large conformational fluctuations of Asp191 were also confirmed by the significantly lower NOE value in comparison with the rest of the protein. This residue is positioned between α-helices 2 and 3, and according to a secondary structure population analysis (Fig. 2), it interchanges between the coil and α-helical secondary structure conformation.

From the ^{15}N R_2 measurements, we found that residues 161–165 in the α1–β2 loop have R_2 rates indicative of chemical exchange in this region. The α1–β2 loop is positioned in the proximity of α-helix 7, and in many X-ray structures this region is coupled to α-helix 7 by hydrophobic interactions between residues Leu161 and Ile306. This coupling might reflect the breathing motion of α-helix 7 that was previously detected in the hydrogen/deuterium exchange experiment,[32] although it could also be an artifact of the proximity of the α1–β2 loop to the disordered C-terminus of the I-domain. Apart from residues in the α1–β2 loop, the majority of other residues with unusually high or low R_2/R_1 values are positioned either in the loop regions or interact with these loop regions. However, two outliers, residues Lys155 and Asp297 that belong to α-helix 1 and α-helix 7, respectively, were detected. Interestingly, these two residues are positioned at the kinks of the two α-helices according to the secondary shift analysis. The chemical exchange of residue Asp297 might be a cause of the breathing motion of α-helix 7 on the timescale of the R_2 measurement.

The dynamics of the I-domain were further explored on the slower timescale by measuring the

Table I. *Parameters Used for the ^{15}N Relaxation Experiments*

Experiment	Pulse sequence	Number of scans	Number of dummy scans	Channel	Channel center (ppm)	Spectral width (ppm)	Number of increments	Data acquisition method
R_1	hsqct1etf3gpsi	8	32	^{1}H	Water signal	13.95	—	Digital quadrature
				^{15}N	119	32	128	Echo–antiecho
R_2	hsqct2etf3gpsi	8	32	^{1}H	Water signal	13.95	—	Digital quadrature
				^{15}N	119	32	128	Echo–antiecho
^{15}N-^{1}H NOE	hsqcnoef3gpsi	32	16	^{1}H	Water signal	13.95	—	Digital quadrature
				^{15}N	119	32	256	Echo–antiecho

backbone amide RDCs. Validation of the X-ray structures in the closed apo, closed inhibitor-bound, intermediate, and open conformation unequivocally suggests that the conformation of α-helix 7 cannot be described with any of the currently available X-ray structures of the LFA-1 I-domain. Similar results were reported for the back calculated RDCs of α-helix 7 from the only NMR structure of the LFA-1 I-domain.[32] On the other hand, we have shown that the RDCs of allosterically coupled MIDAS residues are in better agreement with the back-calculated RDC values, except in the case of the open active conformations. This is a consequence of the MIDAS site rearrangements in the open active conformation necessary for high-affinity ligand binding. We anticipate that the use of multi-state relaxation–dispersion measurements will further clarify the dynamical behavior of the LFA-1 I-domain in particular by allowing accurate exchange rate measurements.

Taken together, the results that we have reported suggest the importance of the low-frequency motions of the LFA-1 I-domain in the inactive apo-state. Among the structural elements, we have identified α-helix 7 as being highly dynamic on the millisecond timescale, although less so on the nanosecond timescale. The RDC measurements indicate that the true position of this α-helix in the closed apo-state can neither be explained by any of the existing X-ray structures nor by individual NMR structures, as it is in a dynamic exchange between many conformations. The conformational fluctuations of α-helix 7 can be described as an inherent property of the I-domain, which might be relevant for controlling the access to the allosteric binding pocket as well as for the downward displacement of α-helix 7 that is necessary in the activation of LFA-1.

Materials and Methods

Expression and purification of the LFA-1 I-domain

^{15}N isotropically labeled LFA-1 I-domain residues 127–311 (GenScript, UK) were expressed from pET-17b vector (Novagen, UK) in *E. coli* BL21(DE3) cells (Invitrogen, UK) by growth in the M9 minimal medium supplemented with 3 g/L $^{15}NH_4Cl$. The protein was purified following the procedure by Legge *et al.*[32] After completion of the procedure, the identity of the protein was confirmed by electrospray mass spectrometry, which showed that the N-terminal methionine had been cleaved.

NMR sample conditions

An NMR sample was prepared in a buffer containing 10 m*M* sodium phosphate (pH 7.2), 0.05% (w/v) NaN_3, 10% D_2O, 10 m*M* $MgSO_4$, and the ^{15}N enriched LFA-1 I-domain at a concentration of 0.1 m*M*. NMR data were initially collected using the ^{1}H-^{15}N HSQC detection scheme on a Bruker Avance 500 MHz Triple Resonance Inverse Spectrometer at 298 K. The ^{15}N-^{1}H chemical shifts were assigned using the previously deposited assignments for the LFA-1 I-domain (BMRB, entry 4553).[32]

^{15}N relaxation experiments

Experimental parameters used to measure the ^{15}N relaxation rate constants are summarized in Table I. The backbone amide ^{15}N R_1, R_2, and ^{15}N-^{1}H heteronuclear NOE relaxation rates were measured on a Bruker Avance Ultrashield Spectrometer with TXI cryoprobe operating at a ^{1}H Larmor frequency of 700.03 MHz and a Bruker Avance Triple Resonance Inverse Spectrometer operating at a ^{1}H Larmor frequency of 500.13 MHz. In each case, the measurements were made at 298 K. The data were processed on Topspin 2.0 with extensive zero filling.

For the R_1 and R_2 measurements, a recycle delay of 2 s (1.8 s for R_1 measurements at 700 MHz) was used between the transients; for the NOE measurements, this value was 5 s. During the R_2 measurements, the CPMG refocusing pulses in the relaxation delay caused sample heating. Therefore, heat-compensating pulses were applied in the beginning of each R_2 experiment so that the same refocusing pulse lengths were used in each relaxation experiment. The relaxation delays in both R_1 and R_2 pulse sequences together with the corresponding heat-compensating pulse lengths were similar to those reported in Ref. 44 and are listed in Table II. Relaxation curves corresponding to the spectra

Table II. *Relaxation Delays for T_1 and T_2 Measurements and Corresponding Heat Compensating Times Used for T_2 Measurements*

Experiment number	Relaxation delay for T_1 (s)	Relaxation delay for T_2 (s)	Heat compensating time for T_2 (s)
1	0.1	0.017	0.272
2	0.8	0.136	0.119
3	1.2	0.255	0.238
4	1.6	0.034	0.255
5	0.2	0.170	0.119
6	1.4	0.068	0.221
7	0.4	0.289	0.000
8	0.1	0.051	0.238
9	0.4	0.204	0.085
10	1.0	0.106	0.183
11	1.4	0.017	0.272
12	0.2	0.068	0.221
13	0.6	0.136	0.153
14	0.3	0.034	0.255

recorded for different delays were fitted using Sparky (version 3.114, UCSF), and relaxation rate constants were obtained from the least-square exponential fitting procedure. Errors were estimated based on repeated determination of the relaxation rate constants by adding random Gaussian noise to each peak in the spectra. The ^{15}N-^{1}H heteronuclear NOE experiment was carried out by the method proposed in Ref. 32.

Model-free analysis

The amplitudes and timescales of the intramolecular motions of the I-domain of LFA-1 were determined from the relaxation measurements by using the model-free formalism.[45–47] For the selection of the dynamical model describing internal motions in a residue-specific manner, a standard numerical optimization procedure[37] was used. Model-free parameters were determined from relaxation data by simultaneously fitting the R_1, R_2, and NOE values obtained at 500 and 700 MHz using the Modelfree4 software (version 4.20).[36] An initial estimate of the overall rotational correlation time, $\tau_m = 12.2$ ns, was obtained from the 10% trimmed average of R_2/R_1 (Ref. 33) and was optimized later. The R_2/R_1 values corresponding to individual residues were similar throughout the protein suggesting isotropic motion. A grid search was used to obtain initial guesses of the other model parameters. After the fitting procedure, the best model for each individual residue was selected following the *F*-statistics-based procedure.[37] Statistical properties of the model-free parameters were calculated from Monte Carlo simulations using 200 randomly distributed synthetic datasets.[36] The results were obtained assuming both axially symmetric and isotropic rotational diffusion. The fitted values of the model-free parameters were almost identical for both isotropic and axially symmetric models, and only the results from the isotropic diffusion model are reported here.

Residual dipolar coupling measurements

For the measurement of ^{15}N-^{1}H RDCs, bacteriophage *Pf1* magnetic resonance cosolvent containing 10 m*M* potassium phosphate at pH 7.6, 2 m*M* $MgCl_2$, and 0.05% NaN_3 was used (Asla Biotech, Lavita).[39] The concentration of *Pf1* in the stock solution was 50 mg/mL. About 55 μL of the *Pf1* stock solution was added to the ^{15}N-enriched LFA-1 I-domain sample in the NMR buffer, resulting in a final protein concentration of 100 μ*M* and a final volume of 160 μL. The sample was then kept at 4°C for 3 h allowing the bubbles to float to the top. Next, the sample was centrifuged at 3000 rpm for 1 min to remove the *Pf1* precipitates. Finally, the sample was transferred into a 3-mm NMR tube and kept at 4°C for another 3 h to let the bubbles float to the top. The ^{15}N-^{1}H RDCs were measured on a Bruker Avance 700 MHz Ultrashield with TXI cryoprobe.

The measured ^{15}N-^{1}H RDCs were back calculated from the previously determined crystal and solution structures using singular value decomposition to fit the alignment tensor. The quality of the agreement with the experimental RDC values was assessed by calculating the quality factor (*Q*-factor) as follows:

$$Q = \frac{\sqrt{\sum \left(\mathrm{RDC}_{\mathrm{calc}} - \mathrm{RDC}_{\mathrm{exp}}\right)^2}}{\sqrt{\sum \left(\mathrm{RDC}_{\mathrm{exp}}\right)^2}}. \quad (1)$$

REFERENCES

1. Barczyk M, Carracedo S, Gullberg D (2010) Integrins. Cell Tissue Res 339:269–280.
2. Hynes R (2002) Integrins: bidirectional, allosteric signaling machines. Cell 110:673–687.
3. Ley K, Laudanna C, Cybulsky M, Nourshargh S (2007) Getting to the site of inflammation: the leukocyte adhesion cascade updated. Nat Rev Immun 7:678–689.
4. Shattil S, Kim C, Ginsberg M (2010) The final steps of integrin activation: the end game. Nat Rev Mol Cell Biol 11:288–300.
5. Takada Y, Ye X, Simon S (2007) The integrins. Genome Biol 8:215.
6. Humphries J, Byron A, Humphries M (2006) Integrin ligands at a glance. J Cell Sci 119:3901–3903.
7. Hynes R (2009) The extracellular matrix: not just pretty fibrils. Science 326:1216–1219.
8. Kishimoto T, Larson R, Corbi A, Dustin M, Staunton D, Springer T. Leukocyte integrins. In: (1988) Structure, function and regulation of molecules involved in leukocyte adhesion. T .A. Springer D. C. Anderson, A.S. Rosenthal R. Rothlein, Editors, Titisee, Germany: Springer.
9. Larson R, Springer T (1990) Structure and function of leukocyte integrins. Immun Rev 114:181–217.
10. Shimaoka M, Takagi J, Springer T (2002) Conformational regulation of integrin structure and function. Ann Rev Biophys Biomol Struct 31:485–516.

11. Dustin M, Springer T (1989) T-cell receptor cross-linking transiently stimulates adhesiveness through LFA-1. Nature 341:619–624.
12. Shimaoka M, Lu C, Palframan R, von Andrian U, McCormack A, Takagi J, Springer T (2001) Reversibly locking a protein fold in an active conformation with a disulfide bond: integrin αL I domains with high affinity and antagonist activity. Proc Natl Acad Sci USA 98: 6009–6014.
13. Zhang H, Liu J-H, Yang W, Springer T, Shimaoka M, Wang J-H (2009) Structural basis of activation-dependent binding of ligand-mimetic antibody AL-57 to integrin LFA-1. Proc Natl Acad Sci USA 106:18345–18350.
14. Luo B-H, Carman C, Springer T (2007) Structural basis of integrin regulation and signaling. Ann Rev Immunol 25:619–647.
15. Campbell I, Humphries M (2011) Integrin structure, activation, and interactions. Cold Spring Harb Perspect Biol 3:pii:a004994.
16. Randi A, Hogg N (1994) I domain of β2 integrin lymphocyte function-associated antigen-1 contains a binding site for ligand intercellular adhesion molecule-1. J Biol Chem 269:12395–12398.
17. Edwards C, Fisher K, Presta L, Bodary S (1998) Mapping the intercellular adhesion molecule-1 and −2 binding site on the inserted domain of leukocyte function-associated antigen-1. J Biol Chem 273:28937–28944.
18. Huang C, Springer T (1995) A binding interface on the I domain of lymphocyte function-associated antigen-1 (LFA-1) required for specific interaction with intercellular adhesion molecule 1 (ICAM-1). J Biol Chem 270: 19008–19016.
19. Champe M, McIntyre B, Berman P (1995) Monoclonal antibodies that block the activity of leukocyte function-associated antigen 1 recognize three discrete epitopes in the inserted domain of CD11a. J Biol Chem 270: 1388–1394.
20. Astrof N, Salas A, Shimaoka M, Chen JF, Springer T (2006) Importance of force linkage in mechanochemistry of adhesion receptors. Biochemistry 45:15020–15028.
21. Lee J-O, Bankston LA, Arnaout A, Liddington R (1995) Two conformations of the integrin A-domain (I-domain): a pathway for activation? Structure 3:1333–1340.
22. Shimaoka M, Xiao T, Liu J-H, Yang Y, Dong Y, Jun C-D, McCormack A, Zhang R, Joachimiak A, Takagi J, Wang J-H, Springer T (2003) Structures of the αL I domain and its complex with ICAM-1 reveal a shape-shifting pathway for integrin regulation. Cell 112:99–111.
23. Qu A, Leahy D (1995) Crystal structure of the I-domain from the CD11a/CD18 (LFA-1, αL β2) integrin. Proc Natl Acad Sci USA 95:10277–10281.
24. Kallen J, Welzenbach K, Ramage P, Geyl D, Kriwacki R, Legge G, Cottens S, Weitz-Schmidt G, Hommel U (1999) Structural basis for LFA-1 inhibition upon lovastatin binding to the CD11a I-domain1. J Mol Biol 292: 1–9.
25. Wattanasin S, Kallen J, Myers S, Guo Q, Sabio M, Ehrhardt C, Albert R, Hommel U, Weckbecker G, Welzenbach K, Weitz-Schmidt G (2005) 1,4-Diazepane-2,5-diones as novel inhibitors of LFA-1. Bioorg Med Chem Lett 15:1217–1220.
26. Crump M, Ceska T, Spyracopoulos L, Henry A, Archibald S, Alexander R, Taylor R, Findlow S, O'Connell J, Robinson M, Shock A (2004) Structure of an allosteric inhibitor of LFA-1 bound to the I-domain studied by crystallography, NMR, and calorimetry. Biochemistry 43:2394–2404.
27. Weitz-Schmidt G, Welzenbach K, Dawson J, Kallen J (2004) Improved lymphocyte function-associated antigen-1 (LFA-1) inhibition by statin derivatives. J Biol Chem 279:46764–46771.
28. Zhang H, Astrof N, Liu J-H, Wang J-H, Shimaoka M (2009) Crystal structure of isoflurane bound to integrin LFA-1 supports a unified mechanism of volatile anesthetic action in the immune and central nervous systems. FASEB J 23:2735–2740.
29. Qu A, Leahy D (1996) The role of the divalent cation in the structure of the I domain from the CD11a/CD18 integrin. Structure 4:931–942.
30. Li S, Wang H, Peng B, Zhang M, Zhang D, Hou S, Guo Y, Dinga J (2009) Efalizumab binding to the LFA-1 αL I domain blocks ICAM-1 binding via steric hindrance. Proc Natl Acad Sci USA 106:4349–4354.
31. Zhang H, Casasnovas J, Jin M, Liu J-H, Gahmberg C, Springer T, Wang J-H (2008) An unusual allosteric mobility of the C-terminal helix of a high-affinity αL integrin I domain variant bound to ICAM-5. Mol Cell 31:432–437.
32. Legge G, Kriwacki R, Chung J, Hommel U, Ramage P, Case D, Dyson J, Wright P (2000) NMR solution structure of the inserted domain of human leukocyte function associated antigen-1. J Mol Biol 295:1251–1264.
33. Kay L, Torchia D, Bax A (1989) Backbone dynamics of proteins as studied by 15N inverse detected heteronuclear NMR spectroscopy: application to Staphylococcal nuclease. Biochemistry 28:8972–8979.
34. Jin M, Song G, Carman C, Kim Y-S, Astrof N, Shimaoka M, Wittrup D, Springer T (2006) Directed evolution to probe protein allostery and integrin I domains of 200,000-fold higher affinity. Proc Natl Acad Sci USA 103:5758–5763.
35. Camilloni C, De Simone A, Vranken W, Vendruscolo M (2012) Determination of secondary structure populations in disordered states of proteins using nuclear magnetic resonance chemical shifts. Biochemistry 51: 2224–2231.
36. Palmer A, Rance M, Wright P (1991) Intramolecular motions of a zinc finger DNA-binding domain from Xfin characterized by proton-detected natural abundance carbon-13 heteronuclear NMR spectroscopy. J Am Chem Soc 113:4371–4380.
37. Mandel A, Akke M, Palmer A (1995) Backbone dynamics of *Escherichia coli* ribonuclease HI: correlations with structure and function in an active enzyme. J Mol Biol 246:144–163.
38. Tolman J, Al-Hashimi H, Kay L, Prestegard J (2001) Structural and dynamic analysis of residual dipolar coupling data for proteins. J Am Chem Soc 123:1416–1424.
39. Hansen M, Mueller L, Pardi A (1998) Tunable alignment of macromolecules by filamentous phage yields dipolar coupling interactions. Nat Struct Biol 5:1065–1074.
40. Losonczi J, Andrec M, Fischer M, Prestegard J (1999) Order matrix analysis of residual dipolar couplings using singular value decomposition. J Magn Reson 138:334–342.
41. Bax A (2003) Weak alignment offers new NMR opportunities to study protein structure and dynamics. Protein Sci 12:1–16.
42. Cabañas C, Hogg N (1993) Ligand intercellular adhesion molecule 1 has a necessary role in activation of integrin lymphocyte function-associated molecule 1. Proc Natl Acadi Sci USA 90:5838–5842.

43. Stewart M, Hogg N (1996) Regulation of leukocyte integrin function: affinity vs. avidity. J Cell Biochem 61:554–561.
44. Farrow N, Muhandham R, Singer A, Pascal S, Kay C, Gish G, Shoelson S, Pawson T, Forman-Kay J, Kay L (1994) Backbone dynamics of a free and a phosphopeptide-complexed Src homology 2 domain studied by 15N NMR relaxation. Biochemistry 33: 5984–6003.
45. Lipari G, Szabo A (1982) Model-free approach to the interpretation of nuclear magnetic resonance relaxation in macromolecules. I. Theory and range of validity. J Am Chem Soc 104:4546–4559.
46. Lipari G, Szabo A (1982) Model-free approach to the interpretation of nuclear magnetic resonance relaxation in macromolecules. II. Analysis of experimental results. J Am Chem Soc 104:4559–4570.
47. Clore M, Szabo A, Bax A, Kay L, Driscoll P, Gronenborn A (1990) Deviations from the simple two-parameter model-free approach to the interpretation of nitrogen-15 nuclear magnetic relaxation of proteins. J Am Chem Soc 112:4989–4991.